Available online at www.sciencedirect.com

ScienceDirect

Mendeleev Commun., 2024, **34**, 316–320

Mendeleev Communications

New ethynediyl-linked perylene diimide/2,1,3-benzothiadiazole conjugates as electron transporting materials for perovskite solar cells

Sergei A. Kuklin,*[a,b] Sergey V. Safronov,[a] Aleksander S. Peregudov,[a] Ekaterina A. Khakina,[a,c] Maria M. Babaskina,[a,c] Marina G. Ezernitskaya,[a] Oleg Yu. Fedorovskii,[a] Elena S. Kobeleva,[d] Leonid V. Kulik,[d] Lyubov A. Frolova,[b] Pavel A. Troshin[b,e] and Aleksey R. Khokhlov[a]

[a] *A. N. Nesmeyanov Institute of Organoelement Compounds, Russian Academy of Sciences, 119334 Moscow, Russian Federation. E-mail: ineos-50@mail.ru*
[b] *Federal Research Center of Problems of Chemical Physics and Medicinal Chemistry, Russian Academy of Sciences, 142432 Chernogolovka, Moscow Region, Russian Federation*
[c] *National Research University Higher School of Economics (HSE University), 101000 Moscow, Russian Federation*
[d] *V. V. Voevodsky Institute of Chemical Kinetics and Combustion, Siberian Branch of the Russian Academy of Sciences, 630090 Novosibirsk, Russian Federation*
[e] *Zhengzhou Research Institute, Harbin Institute of Technology, Jinshui District, 450003 Zhengzhou, China*

DOI: 10.1016/j.mencom.2024.04.003

Two new compounds BT-PDI and BT2-PDI2 were synthesized by the Sonogashira reaction between 4,7-diethynyl-2,1,3-benzothiadiazole and bromoperylene diimide derivatives. The HOMO and LUMO energy levels estimated by UV-VIS spectroscopy and cyclic voltammetry were –5.66/–3.75 and –5.33/–3.41 eV for the BT-PDI and BT2-PDI2, respectively; both compounds form high-quality and smooth coatings on the perovskite surface with the root mean square roughness values 5.95 and 7.80 nm for the BT-PDI and BT2-PDI2 films, respectively; the electron mobilities in the solid films estimated by photo-CELIV method are equal to 5.0×10^{-5} and 3.0×10^{-5} cm^2 V^{-1} s^{-1}, respectively. Both compounds being tested as electron transport layers in perovskite solar cells showed efficiency values of 14.44 and 13.01% for BT-PDI and BT2-PDI2, respectively.

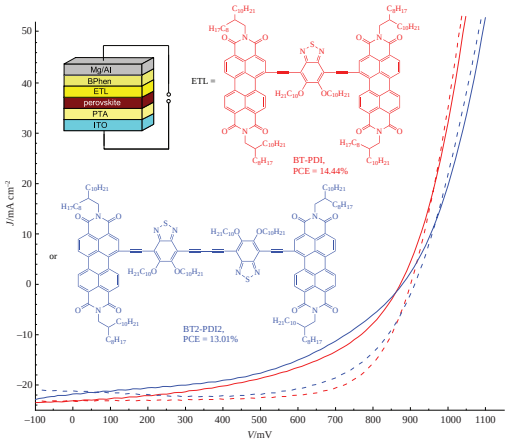

Keywords: Sonogashira reaction, perylene diimide, 2,1,3-benzothiadiazole conjugates, alkynes, electron transport materials, perovskite solar cells, power conversion efficiency.

Currently, perovskite solar cells (PSCs) are the most promising devices for converting sunlight into electricity, with efficiency comparable to crystalline silicon solar cells.[1] In addition to the high power conversion efficiency (PCE), reaching 26.1%,[1] other advantages of PSCs are the ease of production using a large number of different methods for forming active layers from solutions,[2] low sensitivity to impurities,[3] and the possibility of creating devices on flexible polymer substrates.[4] The main disadvantage of PSCs is their short service life due to the instability of the perovskite layer to environmental factors, namely, humidity and oxygen, as well as exposure to sunlight.[5] The efficiency and stability of PSCs are greatly influenced by the charge transport layers, hole transport (HTL) and electron transport layers (ETL) located between the active perovskite layer and the metal electrodes. Proper selection of charge transport layers can improve the extraction of photogenerated charge carriers, reduce recombination and increase the stability of perovskite solar cells.[6]

Perylene diimide (PDI) derivatives have attracted the close researchers' attention due to their low energy levels and strong intermolecular π-stacking, they have high electron mobility, which makes them promising electron transport materials for organic electronics devices.[7] The combination of PDI fragments with other heteroaromatic structural blocks allows the synthesis of a variety of new molecules with the donor–acceptor (D–A) structure, whose optical and electronic properties can be tuned by the appropriate selection of the structure of additional structural blocks.[8,9] Long-term studies have shown that the type of connection of two or more PDI fragments into a single molecule has a great influence on the molecular geometry, optical properties, morphology of the resulting films, molecular packing and photovoltaic efficiency.[10] In particular, the formation of a single σ bond between PDI and any other aromatic fragment leads to highly twisted structures, in which the angle between the planes of the structural fragments falls in the range of 40–90°.[9,11] Obviously, this structural feature can prevent the self-organization of molecules through intermolecular π-stacking interactions, which reduces crystallinity and deteriorates charge transport properties. At the same time, flat structures are the most favorable for good charge mobility, thus there is a reason to suppose that flat aromatic molecules bearing PDI fragments can be interesting materials for organic electronics.

One of the ways to design PDI compound of D–A type with a high degree of molecular planarity is the use of π-ethyne-1,2-diyl bridges connecting the central structural fragments and terminal PDI groups. Several PDI compounds of this type have previously been reported in the literature, which have been used as non-fullerene acceptors in organic and polymer solar cells.[12–18] However, there are currently no examples of using this type of compounds as components of perovskite solar cells.

In the course of our research on the synthesis of new promising materials for PSCs, we recently[19] discovered that this type of compounds can act rather effectively as an electron transport layer in perovskite solar cells with the p-i-n architecture. A maximum efficiency level of 14.18% was achieved, which is a promising value for this new class of materials.[19] Since the properties of such type compounds depend on the structure of the central fragment, we decided to continue research in this direction and design similar structures with other types of central fragment.

Herein, we found that the typical Sonogashira cross-coupling of 1-bromo-*N*,*N*′-bis(2-octyldodecyl)perylene-3,4,9,10-tetracarboxy bisimide **1** with 5,6-bis(decyloxy)-4,7-diethynyl-2,1,3-benzothiadiazole **2** in the presence of the catalyst mixture $CuI/PPh_3/PdCl_2(PPh_3)_2$, in addition to the target product BT-PDI, unexpectedly led to the formation of a significant amount of the by-product BT2-PDI2, which is a product of oxidative dimerization of intermediate **A** (Scheme 1). It should be noted that only a couple of examples of a similar type of perylene diimide conjugates was previously documented,[20] but they were prepared in low yields using oxidative dimerization of the corresponding acetylene monomer.

New compounds BT-PDI and BT2-PDI2 were separated by chromatography and isolated in 47 and 19% yields as black powders, highly soluble in organic solvents such as THF, chloroform, chlorobenzene and toluene. Their ^{1}H NMR spectra show sets of broadened signals with the chemical shifts typical for the fragments present in the molecules (see Online Supplementary Materials, Figures S1–S3). In particular, broadened signals for terminal PDI groups are located at δ 10.50–10.70 and 8.00–8.80 ppm; the signals for methylene groups connected to the oxygen atoms of the benzothiadiazole (BT) fragment and to the nitrogen atoms of the PDI fragments are located at δ 4.60–4.90 and 4.00–4.30 ppm, respectively. The remaining signals of aliphatic substituents are in the range of δ 2.70–2.25 ppm, and the integral intensities of all signals correlate well with the number of structurally nonequivalent protons. The broadening of signals in the ^{1}H NMR spectra can be associated with either the hindered rotation of bulky PDI fragments around single σ bonds, or with the aggregation of molecules in solution.

In the ^{13}C NMR spectra, the signals of carbonyl groups are observed at δ 163.50–162.00 ppm (two signals can overlap in the case of BT2-PDI2); signals of BT fragment are located at δ 158.50–159.30, 151.20–151.10 and 106.44–106.39 ppm (two signals can overlap in the case of BT2-PDI2); the signals of carbon atoms at δ 102.54 and 95.43 ppm, or at δ 102.15, 95.21, 86.36 and 78.29 ppm correspond to the carbon atoms of ethyne-1,2-diyl bridge in the BT-PDI and BT2-PDI2 molecules, respectively. The MALDI-TOF spectra show peaks at *m/z* 2396.222 and 2891.692, corresponding to the proposed structures of BT-PDI and BT2-PDI2, respectively. Additionally, the structures were confirmed by elemental analysis.

We studied optical properties of the new compounds. Interestingly, in chloroform solution the dimeric compound BT2-PDI2 has significantly more intense light absorption over the entire visible range compared to BT-PDI [Figure 1(*a*)]. Simultaneously, at 270–350 nm there are intense absorption bands of triple bonds, and in the region of 380–650 nm the absorption bands of the central structural block and side PDI groups are localized.[13]

For both compounds in solution, the spectra are well resolved in the visible region and contain several main clearly visible

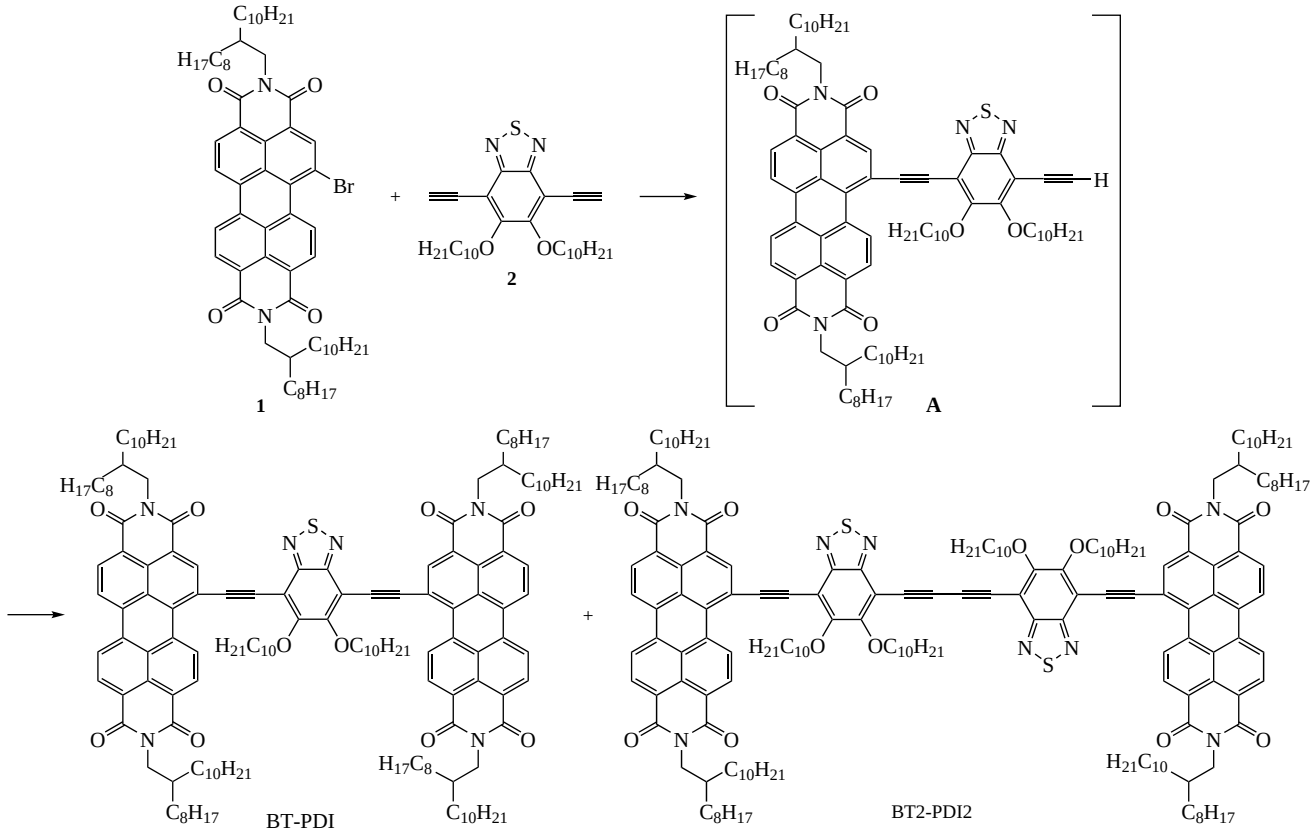

Scheme 1 *Reagents and conditions*: $PdCl_2(PPh_3)_2$, CuI, PPh_3, THF/NEt_3, 78 °C, 48 h.

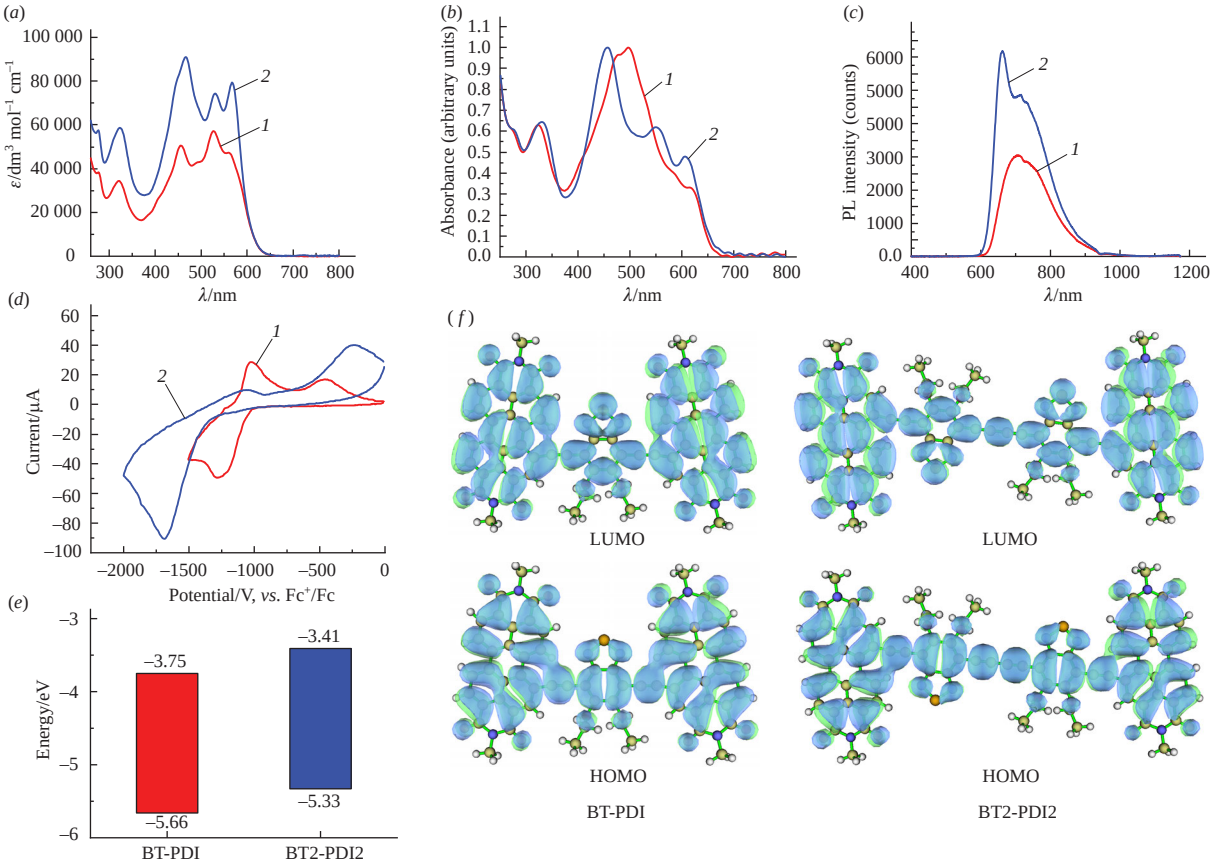

Figure 1 UV-VIS spectra (*a*) in chloroform solution and (*b*) in films, (*c*) photoluminescence spectra in films, (*d*) cyclic voltammograms of film, (*e*) energy level diagram and (*f*) calculated HOMO/LUMO distributions of compounds BT-PDI (*1*) and BT2-PDI2 (*2*).

absorption bands corresponding to electronic transitions from the ground state to some vibrational levels of the excited state. It seems that the main band corresponding to the 0–0 transition is the band with a maximum at 527 and 530 nm for BT-PDI and BT2-PDI2, respectively. These values are close to the positions of the absorption band maxima corresponding to 0–0 transitions in individual PDI fragments (528 nm).[21,22] Additional long-wave bands at 561 nm (BT-PDI) and 564 nm (BT2-PDI2) presumably correspond to the formation of *J*-aggregates of molecules in solution.[17] Upon the transition from solution to solid state, most vibrational bands undergo broadening and largely overlap with the main 0–0 transition band [Figure 1(*b*)]. This fact, together with the shift of absorption edge to longer wavelengths, indicates higher intermolecular association upon transition from solution to films. The bathochromic shift of the absorption edge is 33 and 47 nm, and the optical band gap (E_g^{opt}) values determined from Tauc plots (Figures S4 and S5) are almost equal, 1.91 and 1.92 eV, for the BT-PDI and BT2-PDI2 compounds, respectively (Table 1). The photoluminescence (PL) spectrum of BT-PDI films contains a broad band with a maximum at 707 nm and a shoulder at 730 nm; in the case of BT2-PDI2 there are bands at 663 and 715 nm [Figure 1(*c*)], and for BT2-PDI2 the luminescence intensity is much higher. The energies of the lowest unoccupied molecular orbitals (LUMO) were estimated using cyclic voltammetry (CVA) of films [see Figure 1(*d*),(*e*), Figures S4, S5 and Table 1] and amount to –3.75 and –3.41 eV for BT-PDI and BT2-PDI2, respectively. The corresponding energy values of the highest occupied molecular orbitals (HOMO) are –5.66 and –5.33 eV. In general, for the dimeric compound BT2-PDI2, the HOMO/LUMO energy values are 0.33–0.34 eV higher than the corresponding values for BT-PDI, which can be explained by the electron-donating effect of two additional triple bonds in the structure of the BT2-PDI2 molecule.

According to the DFT calculations, the molecules of both compounds have a high degree of planarity (Figures S6 and S7) because, thanks to the ethyne-1,2-diyl bridges, the bulky terminal PDI groups are not particularly constrained to rotate around single σ-bonds, allowing the molecules to achieve planar conformation. This should favor an increase in the crystallinity in the films and contribute to an increase in the charge-transport properties of materials based on these molecules. The rotation angles of PDI fragments relative to the planes of the central BT fragments are 8.80–8.95° in the BT-PDI molecule and 6.06–8.35° in the BT2-PDI2 structure, respectively; moreover, the two BT fragments in the BT2-PDI2 molecule lie almost in the same plane, *i.e.* the calculated angle of rotation relative to each other is no more than 1.05°. The HOMO/LUMO distribution within both molecules is quite uniform [Figure 1(*f*) and Figures S6, S7], and their calculated energies are −5.94/−3.85 and −5.82/−3.79 eV

Table 1 Optical and electronic properties of compounds BT-PDI and BT2-PDI2.

Compound	$\lambda^{abs}_{max\ film}$/nm[a]	λ^{abs}_{onset}/nm	E_g^{opt}/eV[b]	E_{LUMO}/eV[c]	E_{HOMO}/eV[d]	E^T_{HOMO}/eV[e]	E^T_{LUMO}/eV[e]	μ_e^f/cm² V⁻¹ s⁻¹
BT-PDI	615, 497, 479, 323	658	1.91	-3.75	–5.66	–5.94	–3.85	5.0×10^{-5}
BT2-PDI2	606, 550, 457, 330, 274	658	1.92	-3.41	–5.33	–5.82	–3.79	3.0×10^{-5}

[a] Cast from $CHCl_3$ solution. [b] $E_g^{opt} = 1240/\lambda_{onset,film}$. [c] $E_{LUMO} = -e(\varphi_{red} + 4.80)$/eV, where φ_{red} is reduction potential, 0.1 M Bu_4NPF_6/MeCN, glassy carbon working disc electrode, Ag^+/Ag reference electrode, Pt counter electrode, Fc^+/Fc internal standard, scanning rate 50 mV s⁻¹. [d] $E_{HOMO} = E_{LUMO} - E_g^{opt}$ (eV). [e] Calculated on the B3LYP//6-311g(d,p) level of theory. [f] Determined by photo-CELIV method.

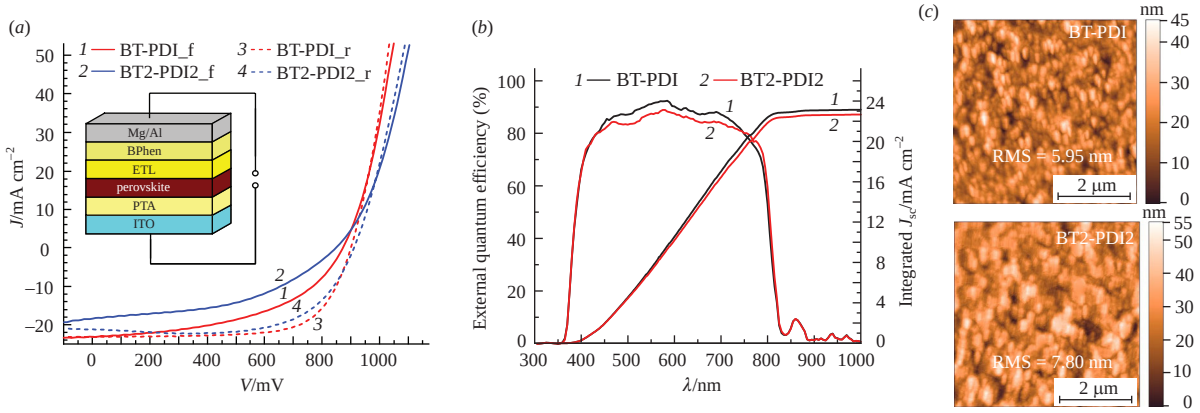

Figure 2 (*a*) Device architecture and *J*–*V* curves, (*b*) EQE spectra of the perovskite solar cells with ETL composed of new compounds BT-PDI and BT2-PDI2, (*c*) and AFM images (5×5 μm^2) of BT-PDI and BT2-PDI2 films on the perovskite surface.

for the BT-PDI and BT2-PDI2 molecules, respectively. It should be noted that there is a noticeable difference between the experimental and calculated values of the HOMO/LUMO energies (see Table 1). The reason for this discrepancy could originate from the fact that the calculations were carried out for isolated molecules in vacuum, and the aggregation effect in the solid state was not taken into account.

We examined the performance of new compounds BT-PDI and BT2-PDI2 as charge transport materials in solar cells with a light-absorbing layer based on cesium/formamidine (Cs/FA) perovskite $Cs_{0.12}FA_{0.88}PbI_3$. For this purpose, we fabricated p-i-n architecture devices with the ITO/PTA/perovskite/BT-PDI or BT2-PDI2/BPhen/Al structure in which indium tin oxide (ITO) acts as a transparent electrode, and poly[bis(4-phenyl)-(4-methylphenyl)amine] (PTA) and BT-PDI or BT2-PDI2 compounds play the role of hole transport and electron transport layers, respectively, and an additional blocking layer of diphenylphenanthroline (BPhen) was applied [Figure 2(*a*)].

The results obtained for devices with both types of electron transporting layers demonstrate promising performance, with maximum power conversion efficiency (PCE) values of 14.44 and 13.01% for BT-PDI- and BT2-PDI2-based devices, respectively [Figure 2(*b*) and Table 2]. The small difference in PCEs values is due to a noticeable difference of the short circuit current density values (J_{sc}), which are equal to 23.13–23.14 and 21.77–21.17 mA cm^{-2} for cells based on BT-PDI and BT2-PDI2, respectively. The open circuit voltage (V_{oc}) values are very close and are equal to 872.52 and 878.25 mV and 900.45 and 911.10 mV for the forward and reverse potential scan directions, while the values differ by no more than 6–11 mV. For both devices, high external quantum efficiency (EQE) (80–90%) is observed across the entire visible wavelength range of 400–750 nm [Figure 2(*c*)]. The values of the integrated short-circuit current determined from the EQE spectra are of 23.14 and 21.84 mA cm^{-2}, and correlate well with the J_{sc} values estimated from the current–voltage characteristics (see Table 2), which also confirms the correctness of the measurements.

Table 2 Photovoltaic parameters of perovskite solar cells with ETL composed of new compounds BT-PDI and BT2-PDI2.

ETL	Scan direction	V_{oc}/mV	J_{sc}/ mA cm^{-2}	FF (%)	PCE (%)	$J_{sc\ EQE}$[a]/ mA cm^{-2}
BT-PDI	F	872.52	23.13	49.31	9.95	23.14
	R	900.45	23.14	69.30	14.44	
BT2-PDI2	F	878.25	21.77	47.62	9.11	21.84
	R	911.10	21.17	67.45	13.01	
PCBM (control)	F	917.57	20.63	78.53	14.86	22.01
	R	925.88	20.71	83.74	16.06	

[a] $J_{sc\ EQE}$ is the short circuit current density calculated by integrating the EQE spectrum over the reference AM1.5G solar emission spectrum.

In order to understand the reasons for the different efficiency of PSCs with different ETLs, we studied the morphological structure of BT-PDI and BT2-PDI2 films deposited on the perovskite surface. Using atomic force microscopy (AFM), we found that both compounds formed high-quality and smooth films on the perovskite. The root mean square (RMS) roughness values are 5.95 and 7.80 nm for the BT-PDI and BT2-PDI2 films, respectively [see Figure 2(*c*)]. These values are far less than for bare perovskite film without any coating where the RMS value of 14.24 nm was observed (Figure S8). Thus, it is clear that the smoothest films were formed in the case of the BT-PDI compound, which can explain the higher PCE of solar cells based on it, since the good morphology of charge-transport layers is one of the key factors influencing the efficiency of solar cells.

Additionally, we estimated the electron mobility values in the films of both compounds, and the values of 5.0×10^{-5} and 3.0×10^{-5} cm^2 V^{-1} s^{-1} were obtained by photo-CELIV method with the device structure ITO/PEDOT-PSS/active layer/PFN/Field's alloy, where active layer is a mixture of regiorandom poly-3-hexylthiophene (*rra*-P3HT) polymer and the compound BT-PDI or BT2-PDI2 (1 : 1, w/w). These values show that the new compounds of this structural type are indeed quite good electron transport materials, and the compound BT-PDI has slightly higher electron mobility in film state, which can explain the higher PCE of solar cells based on it.

In conclusion, two new compounds, monomeric BT-PDI and dimeric BT2-PDI2, were shown to possess good properties for the use in perovskite solar cells. We are currently continuing research and optimization of solar cells based on this interesting type of compounds, aimed at increasing their efficiency and reducing the hysteresis of current–voltage characteristics; the results obtained will be published elsewhere.

This study was funded by the Russian Science Foundation (grant no. 22-23-00318). NMR, MALDI, UV-absorption and cyclic voltammetry studies and elemental analysis were performed with the financial support of the Ministry of Science and Higher Education of the Russian Federation employing the equipment of Center for molecular composition studies of INEOS RAS. Photovoltaic, photoluminescence, and atomic force microscopy studies were performed employing the equipment of Federal Research Center for Problems of Chemical Physics and Medicinal Chemistry of RAS.

Online Supplementary Materials

Supplementary data associated with this article can be found in the online version at doi: 10.1016/j.mencom.2024.04.003.

References

1 *Best Research-Cell Efficiency Chart, Photovoltaic Research*, National Renewable Energy Laboratory (NREL), 2022, https://www.nrel.gov/pv/cell-efficiency.html.
2 N. K. Tailor, M. Abdi-Jalebi, V. Gupta, H. Hu, M. I. Dar, G. Li and S. Satapathi, *J. Mater. Chem. A*, 2020, **8**, 21356.
3 J. R. Poindexter, R. L. Hoye, L. Nienhaus, R. C. Kurchin, A. E. Morishige, E. E. Looney, A. Osherov, J.-P. Correa-Baena, B. Lai and V. Bulovic, *ACS Nano*, 2017, **11**, 7101.
4 S. Aftab, S. Hussain, F. Kabir, M. Aslam, A. H. Rajpar and A. G. Al-Sehemi, *Nano Energy*, 2023, **120**, 109112.
5 A. K. Jena, A. Kulkarni and T. Miyasaka, *Chem. Rev*., 2019, **119**, 3036.
6 M. Cheng, C. Zuo, Y. Wu, Z. Li, B. Xu, Y. Hua and L. Ding, *Sci. Bull*., 2020, **65**, 1237.
7 X. Zhan, A. Facchetti, S. Barlow, T. J. Marks, M. A. Ratner, M. R. Wasielewski and S. R. Marder, *Adv. Mater*., 2011, **23**, 268.
8 F. Fernández-Lázaro, N. Zink-Lorre and Á. Sastre-Santos, *J. Mater. Chem. A*, 2016, **4**, 9336.
9 V. Sharma, J. D. B. Koenig and G. C. Welch, *J. Mater. Chem. A*, 2021, **9**, 6775.
10 Y. Duan, X. Xu, Y. Li and Q. Peng, *Chin. Chem. Lett.*, 2017, **28**, 2105.
11 K. Fang, Y. Huang, G. Chang, J. Yang, Y. Shen and X. Ye, *Macromol. Res*., 2015, **23**, 545.
12 S. Xie, J. Zhang, L. Wu, J. Zhang, C. Li, X. Chen, Z. Wie and Z. Bo, *Dyes Pigm*., 2017, **146**, 143.
13 J. Cann, S. Dayneko, J.-P. Sun, A. D. Hendsbee, I. G. Hill and G. C. Welch, *J. Mater. Chem. C*, 2017, **5**, 2074.
14 Y. Guo, Y. Liu, Q. Zhu, C. Li, Y. Jin, Y. Puttisong, W. Chen, F. Liu, F. Zhang, W. Ma and W. Li, *ACS Appl. Mater. Interfaces*, 2018, **10**, 32454.
15 Y. Liu, G. Liu, R. Xie, Z. Wang, W. Zhong, Y. Li, F. Huang and Y. Cao, *Chem. Mater*., 2018, **30**, 4331.
16 C. Yu, Y. Xu, S. Liang, X. Jiang, G. Feng, C. Li and W. Li, *Chin. Chem. Lett*., 2018, **29**, 325.
17 F. Tang, K. Wu, Z. Zhou, G. Wang, Y. Pei, B. Zhao and S. Tan, *Dyes Pigm.*, 2018, **156**, 276.
18 A. Zhang, C. Li, F. Yang, J. Zhang, Z. Wang, Z. Wei and W. Li, *Angew. Chem., Int. Ed.*, 2017, **56**, 2694.
19 S. A. Kuklin, S. V. Safronov, E. A. Khakina, A. G. Buyanovskaya, L. A. Frolova and P. A. Troshin, *Mendeleev Commun*., 2023, **33**, 314.
20 Y. Shi, H. Wu, L. Xue and X. Li, *J. Colloid Interface Sci.*, 2012, **365**, 172.
21 M. Nazari, E. Cieplechowicz, T. A. Welsh and G. C. Welch, *New J. Chem*., 2019, **43**, 5187.
22 Q. Deng, E. Zhou, Y. Huang, W. Qing, H. Zhai, Z. Liu and Z. Wei, *Chem. Commun*., 2019, **55**, 4379.

Received: 7th December 2023; Com. 23/7336